IL NUOVO CIMENTO Vol. 34 C, N. 4 Luglio-Agosto 2011
DOI 10.1393/ncc/i2011-10948-0

Colloquia: Channeling 2010

# Development of a beamline for the study of interactions between a relativistic electron beam and crystals at the SAGA Light Source

Y. Takabayashi(*), T. Kaneyasu and Y. Iwasaki
*SAGA Light Source - 8-7 Yayoigaoka, Tosu, Saga 841-0005, Japan*

(ricevuto il 22 Dicembre 2010; pubblicato online il 29 Agosto 2011)

**Summary.** — A beamline dedicated to the study of interactions of a relativistic electron beam with crystals has been designed and constructed at the SAGA Light Source (SAGA-LS). This beamline consists of a compact two-axis goniometer in a vacuum chamber and two screen monitors placed downstream of the goniometer. An electron beam is provided from the SAGA-LS injector linac. The beam parameters such as the beam emittance and the Twiss parameters have been measured using the "Q-scan method". Proposals for experiments on channeling radiation and parametric X-ray radiation are also discussed.

PACS 29.20.-c – Accelerators.
PACS 61.85.+p – Channeling phenomena (blocking, energy loss, etc.).

## 1. – Introduction

A variety of radiation phenomena occur during the interaction between relativistic electrons and a crystal. If an electron is incident on the crystal along its axis or plane, channeling radiation (CR) is emitted [1]. Moreover, the so-called parametric X-ray radiation (PXR) is emitted in a direction satisfying the Bragg condition [2]. In order to study such unique radiation phenomena, we have developed a dedicated beamline at the linac room at the SAGA Light Source (SAGA-LS). In this paper, we report the design of this beamline and proposals for experiments on CR and PXR.

## 2. – SAGA Light Source (SAGA-LS)

The SAGA-LS is a synchrotron radiation facility located in Saga prefecture in Japan [3-5]. The construction of the accelerators started in 2003 and the accelerators were commissioned from 2004 to 2005. In 2006, the SAGA-LS officially opened as a source of

(*) E-mail: takabayashi@saga-ls.jp

 

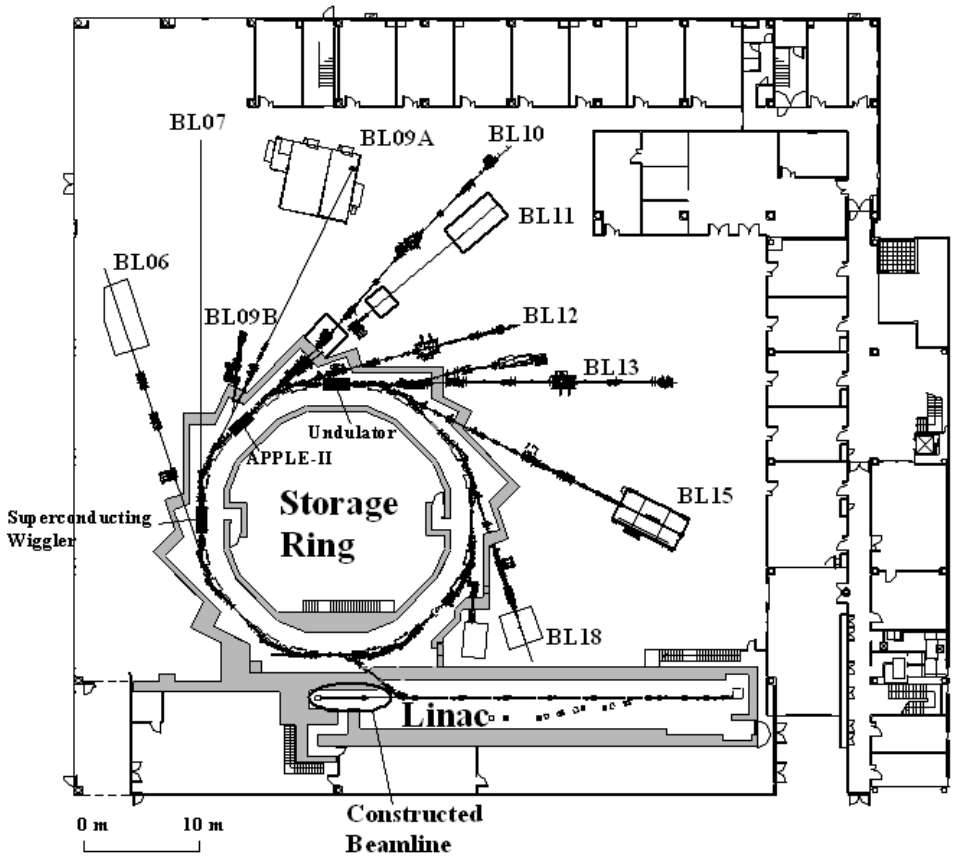


Fig. 1. – Schematic layout of the SAGA-LS facility. The ellipse shows the location of the constructed beamline.

synchrotron radiation (SR). Figure 1 shows a schematic layout of the SAGA-LS facility. The accelerator complex consists of a 255 MeV injector linac and a 1.4 GeV storage ring. The linac is composed of a 100 kV thermionic electron gun, a 714 MHz sub-harmonic buncher, an *S*-band (2856 MHz) standing-wave buncher, and six *S*-band accelerating tubes. After an electron beam is accelerated up to 255 MeV at the linac, the beam is injected into the storage ring with a repetition rate of 1 Hz. In daily operation, electrons are stored up to 300 mA. Next, the electron beam is accelerated to 1.4 GeV in the storage ring and SR from the 1.4 GeV electron beam is produced. At present, there are nine SR beamlines, covering a wide spectrum range from vacuum ultraviolet (VUV) to hard X-rays.

## 3. – Experimental setup

Figure 2 shows a schematic layout of the beamline constructed at the SAGA-LS linac. The location of this beamline is indicated by the ellipse in fig. 1. We modified an existing beamline extending from the linac exit to a beam dump to install a goniometer and two screen monitors.

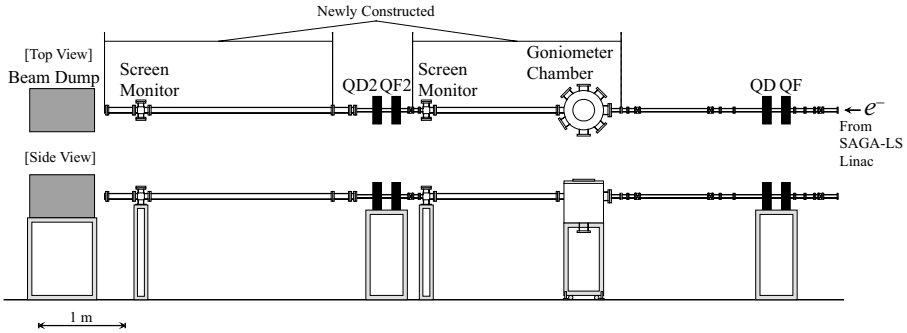


Fig. 2. – Schematic layout of the beamline constructed at the SAGA-LS linac.

Figure 3 shows a schematic drawing of the goniometer. Its specifications are summarized in table I. The horizontal and vertical angular ranges of the goniometer are $-180°$–$+180°$ and $-10°$–$+10°$. The angular step sizes for both axes are sufficiently smaller than the critical angle for channeling. The goniometer is placed on a translational stage and is removable from the beam axis.

We installed the goniometer in a vacuum chamber to avoid multiple scattering in air. Since the goniometer chamber is connected to the linac, the vacuum pressure of the goniometer chamber must be lower than that of the linac ($\sim 10^{-6}$ Pa). In order to achieve this condition, we used a goniometer and a chamber designed for ultrahigh vacuum use. The goniometer and the chamber are bakable at 120 °C and 150 °C, respectively. After installation in the linac, a vacuum pressure of $\sim 1 \times 10^{-6}$ Pa was attained, which is acceptable for the linac vacuum.

We prepared two screen monitors downstream of the goniometer. The angular divergence of a beam transmitted through a target changes depending on the beam energy and the target thickness. In order to cover a wide angular divergence range, we installed the screen monitors at positions near and far from the target. A 0.1 mm thick alumina ($Al_2O_3$) plate was used as a fluorescent screen. The screen was inserted with an air-cylinder actuator. The measured beam size is known to be larger than the real beam size

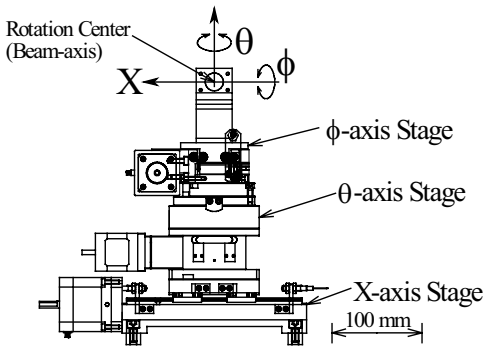


Fig. 3. – Schematic drawing of the goniometer.

TABLE I. – *Specifications of the goniometer.*

| | Range | Minimum step |
|---|---|---|
| $\theta$ | $-180^\circ$–$+180^\circ$ | $0.000069^\circ$ |
| $\phi$ | $-10^\circ$–$+10^\circ$ | $0.000019^\circ$ |
| $X$ | $-50\,\mathrm{mm}$–$+50\,\mathrm{mm}$ | $0.002\,\mathrm{mm}$ |

if a thick screen (for example, 1 mm thick) is used because the fluorescent light emitted inside the screen is broadened due to scattering. In order to suppress this effect, we chose a thin screen. The fluorescent light is detected with a digital CCD camera (black-and-white). The digital data of the two-dimensional image is transferred from the CCD camera to a personal computer via gigabit Ethernet. Recently, we have succeeded in detecting optical transition radiation (OTR) from a Si crystal. We plan to measure the beam profile at the target position utilizing the OTR.

It is known that the profile of an electron beam channeling through a crystal exhibits interesting features [6]. The peak position and peak width of the beam profile change depending on the crystal angle around the channeling condition. Therefore, we can determine the channeling condition by observing the beam profile using the screen monitor. The screen monitor can also be used for measuring beam parameters, as discussed in the next section.

## 4. – Beam parameters

We evaluated the beam emittance and the Twiss parameters using the "Q-scan method". In this method, the beam size is measured as a function of the magnetic strength of a quadrupole magnet. Under our experimental conditions, the transfer matrix of the lattice (magnet arrangement) is given by

$$(1)\qquad M = \begin{pmatrix} m_{11} & m_{12} \\ m_{21} & m_{22} \end{pmatrix} = M_{\mathrm{drift}} M_{\mathrm{QD}} = \begin{pmatrix} 1 & d \\ 0 & 1 \end{pmatrix} \begin{pmatrix} \cosh(\sqrt{K}L) & \frac{1}{\sqrt{K}} \sinh(\sqrt{K}L) \\ \sqrt{K} \sinh(\sqrt{K}L) & \cosh(\sqrt{K}L) \end{pmatrix},$$

where $M_{\mathrm{QD}}$ and $M_{\mathrm{drift}}$ are the transfer matrices of the defocusing quadrupole magnet and the drift space, respectively, $d$ is the length of the drift space, $K$ represents the strength of the quadrupole magnet (the ratio of the magnetic gradient and the magnetic rigidity), and $L$ is the length of the quadrupole magnet [7]. Using this transfer matrix, the Twiss parameters become

$$(2)\qquad \begin{pmatrix} \beta_{\mathrm{f}} \\ \alpha_{\mathrm{f}} \\ \gamma_{\mathrm{f}} \end{pmatrix} = \begin{pmatrix} m_{11}^2 & -2m_{11}m_{12} & m_{12}^2 \\ -m_{11}m_{21} & m_{11}m_{22} + m_{12}m_{21} & -m_{22}m_{12} \\ m_{21}^2 & -2m_{22}m_{21} & m_{22}^2 \end{pmatrix} \begin{pmatrix} \beta_{\mathrm{i}} \\ \alpha_{\mathrm{i}} \\ \gamma_{\mathrm{i}} \end{pmatrix}.$$

Here, $(\beta_{\mathrm{i}}, \alpha_{\mathrm{i}}, \gamma_{\mathrm{i}})$ and $(\beta_{\mathrm{f}}, \alpha_{\mathrm{f}}, \gamma_{\mathrm{f}})$ are the Twiss parameters at the entrance position of the quadrupole magnet and the screen position, respectively. The parameter $\gamma_{\mathrm{i(f)}}$ is defined

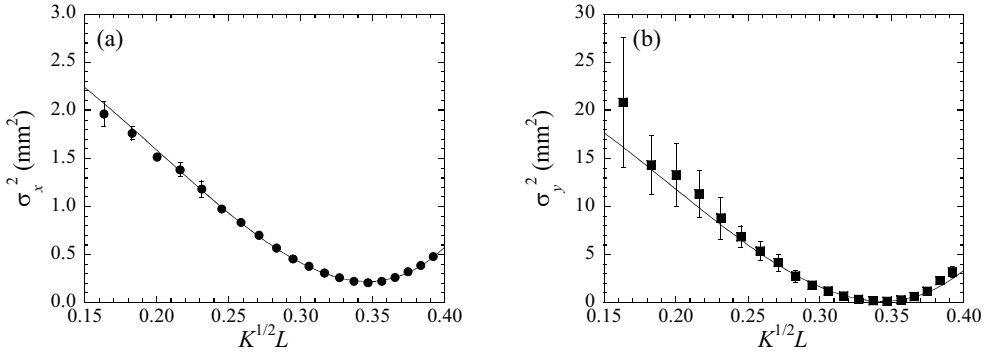


Fig. 4. – Square of the beam size as a function of $K^{1/2}L$. Horizontal (a) and vertical (b). The solid line shows the fit to the experimental data.

as $(1+\alpha_{\mathrm{i(f)}}^2)/\beta_{\mathrm{i(f)}}$. The square of the beam size at the screen position is obtained as

$$\sigma^2 = \varepsilon\beta_{\mathrm{f}} = \varepsilon(m_{11}^2\beta_{\mathrm{i}} - 2m_{11}m_{12}\alpha_{\mathrm{i}} + m_{12}^2\gamma_{\mathrm{i}}), \tag{3}$$

where $\varepsilon$ is the natural emittance.

Figure 4 shows the result of the Q-scan measurement. The beam energy was 255 MeV. We used a defocusing quadrupole magnet (QD) placed upstream of the goniometer (see fig. 2). The beam profile was measured using the upstream screen monitor. The beam size $\sigma$ was extracted by fitting a Gaussian function to the beam profile. The solid line in fig. 4 shows the fit to the experimental data by eq. (3). From this analysis, the natural emittances were determined as $\varepsilon_x = 0.043$ and $\varepsilon_y = 0.100\,\pi$·mm·mrad, and the initial Twiss parameters were obtained as $\beta_{\mathrm{i},x} = 3.5\,\mathrm{m}$, $\alpha_{\mathrm{i},x} = 4.9$, $\beta_{\mathrm{i},y} = 11.8\,\mathrm{m}$, and $\alpha_{\mathrm{i},y} = -11.2$. The subscripts $x$ and $y$ represent the horizontal and vertical quantities, respectively. The normalized emittance, which is a conservative quantity, can be written as $\varepsilon_{\mathrm{n}} = \gamma\varepsilon$ ($\gamma$ is the Lorentz factor); $\varepsilon_{\mathrm{n},x} = 21$ and $\varepsilon_{\mathrm{n},y} = 50\,\pi$·mm·mrad.

We calculated the beam size and beam divergence at the target position as a function of the $K$ value of the quadrupole magnet QD. The result is shown in fig. 5. The natural emittances and the initial Twiss parameters derived above were used in this calculation. The critical angle for planar channeling can be written as

$$\psi_{\mathrm{p}} = \sqrt{\frac{4\pi Z_{\mathrm{t}} e^2 N d_{\mathrm{p}} a_{\mathrm{TF}}}{pv}} = \sqrt{\frac{4\pi Z_{\mathrm{t}} e^2 N d_{\mathrm{p}} a_{\mathrm{TF}}}{\gamma m v^2}}, \tag{4}$$

where $Z_{\mathrm{t}}$ is the target atomic number, $N$ is the atomic number density of the target, $d_{\mathrm{p}}$ is the inter-planar distance, $p$ is the projectile momentum, $v$ is the projectile velocity, and $a_{\mathrm{TF}}$ is the Thomas-Fermi radius. For the planar channeling of 255 MeV electrons in Si(220), the critical angle is calculated to be 0.43 mrad. This critical angle is indicated by the horizontal solid line in fig. 5(b). In the region $\sim 5 < K <\sim 13\,\mathrm{m}^{-2}$, the vertical beam divergence $\sigma_y'$ is smaller than the critical angle; most of the electrons are expected to channel when the channeling plane is horizontal. As shown in eq. (4), the critical angle is proportional to $\gamma^{-1/2}$. The beam divergence is also proportional to $\gamma^{-1/2}$, since the beam divergence depends on the square root of the natural emittance ($\varepsilon = \varepsilon_{\mathrm{n}}/\gamma$). Therefore,

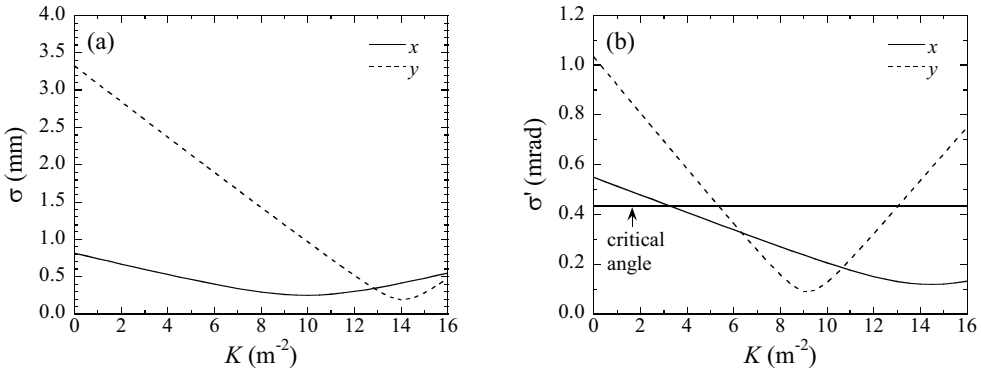


Fig. 5. – Beam size (a) and beam divergence (b) at the target position as a function of $K$. The solid and dotted lines show the horizontal and vertical values, respectively. The horizontal solid line in (b) represents the critical angle for planar channeling.

when the channeling condition is fulfilled at a certain beam energy, this condition is true for other beam energies if we assume that the Twiss parameters are the same.

## 5. – Proposed experiments

We plan to perform two studies using this beamline: i) diffracted channeling radiation (DCR) and ii) PXR from single crystals and polycrystals [8-10]. In this paper, we mainly report on the DCR experiment proposal. The PXR experiment proposal is discussed elsewhere [11].

The DCR process was predicted by Baryshevsky *et al.* in 1983 [12]. Detailed calculations on DCR for planar channeling were performed by Nitta *et al.* in 1996 [13, 14] and 2001 [15]. Moreover, detailed calculations on DCR for axial channeling were recently performed by Korotchenko *et al.* [16,17]. However, DCR has not yet been observed. The DCR process takes place if the CR energy $\hbar\omega_{\mathrm{CR}}$ coincides with the Bragg energy $\hbar\omega_{\mathrm{B}}$:

$$\hbar\omega_{\mathrm{CR}} = \hbar\omega_{\mathrm{B}}. \tag{5}$$

This radiation process can be interpreted as diffraction of "virtual channeling radiation". The CR energy can be written as

$$\hbar\omega_{\mathrm{CR}} \simeq 2\gamma^2(E_{\mathrm{f}} - E_{\mathrm{i}}), \tag{6}$$

where $E_{\mathrm{i}}$ and $E_{\mathrm{f}}$ are the initial and final energy levels for the transverse state of the channeled electron, respectively. Due to relativistic effects, the CR energy is multiplied by $2\gamma^2$. On the other hand, the Bragg energy is given by

$$\hbar\omega_{\mathrm{B}} = \hbar c|\boldsymbol{g}|/(2\sin\theta_{\mathrm{B}}), \tag{7}$$

where $c$ is the light velocity, $\boldsymbol{g}$ is the reciprocal lattice vector, and $\theta_{\mathrm{B}}$ is the Bragg angle. Because the CR energy depends on $\gamma$, both the crystal angle and the beam energy must be controlled to fulfill the DCR condition. This is different from the PXR condition. In ref. [15], some characteristics of the DCR are derived as follows. i) The DCR appears

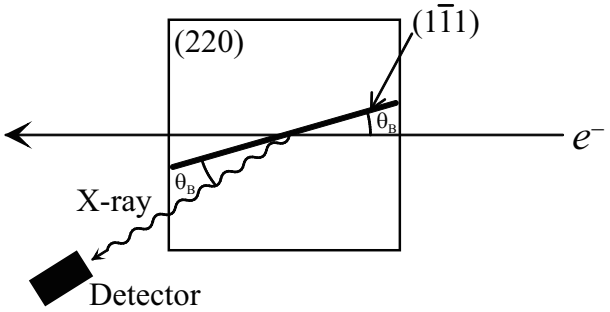


Fig. 6. – Schematic of the DCR experiment. The (220) plane is parallel to the paper surface, and the (1$\bar{1}$1) plane is perpendicular.

around the center of the PXR distribution where the PXR intensity is low. ii) The peak height of the DCR distribution is larger than that of the PXR distribution by about one order of magnitude. iii) The DCR has a threshold for beam energy. If the beam energy is smaller than the threshold, the intensity of the DCR drastically decreases.

A schematic of the DCR experiment is illustrated in fig. 6. This is the same arrangement as that considered in ref. [15] (the beam energy is 10 MeV). A Si crystal is used as a target. The (220) plane is employed as the channeling plane, and the (1$\bar{1}$1) plane as the diffraction plane. The CR energy for the transition from the first excited state to the ground state ($n = 1 \to 0$) is expected to be 7.1 keV, and the Bragg angle $\theta_B = 16.1°$. Using Nitta's formalism, the DCR and PXR yields are estimated to be $\sim 1.5 \times 10^3$ and $\sim 4.6 \times 10^4$ photons/s, respectively, for a beam current of 10 nA (typical current at the SAGA-LS linac), target thickness of 10 $\mu$m, and acceptance angle of the detector of $100 \times 100$ mrad. For simplicity, the beam size and beam divergence at the target were neglected in this estimation. When the acceptance angle is reduced to $10 \times 10$ mrad, the DCR and PXR yields are calculated to be $\sim 1.3 \times 10^3$ and $\sim 6.4 \times 10^1$ photons/s, respectively. Thus, the DCR can be efficiently discriminated from the PXR by restricting the acceptance angle.

As already discussed, the DCR is sensitive to beam energy. We thus propose to apply the DCR phenomenon to beam energy measurement. Substituting eqs. (6) and (7) into eq. (5), we obtain

$$\gamma = \sqrt{\frac{1}{2(E_i - E_f)} \frac{\hbar c |\boldsymbol{g}|}{2 \sin \theta_B}}. \tag{8}$$

Accordingly, the Lorentz factor $\gamma$, *i.e.* the beam energy, can be determined from the Bragg angle $\theta_B$. In this method, the crystal plays the role of a spectrometer as well as a radiator of channeling radiation. In our proposed method, the accuracy of the absolute beam energy measurement depends on two terms: the Bragg angle $\theta_B$ and the transverse transition energy $E_i - E_f$. Since the precision in the rotation angle of the goniometer is sufficiently high, the precision of the absolute beam energy is mainly determined by that of the transition energy. Thus, the precision of the beam energy is estimated to be $\sim 1\%$ [18]. As we are only concerned with the relative beam energy, we can neglect the transition energy term. In this case, the precision of the beam energy is determined by the Bragg angle and is estimated to be $\sim 0.01\%$ [18].

The advantages of this new method of beam energy measurement are as follows. i) Until now, bending magnets have been used as spectrometers for the measurement of electron beam energy. In such spectrometers, the electron beam must be bent and it may be necessary to prepare a beam transport line and a beam dump. In our proposed method, it is possible to measure the beam energy without bending the beam. ii) Because a bending magnet is not used, there are no problems associated with magnet hysteresis. iii) If a mirror-polished crystal is used as a target, we can also measure the beam profile and the bunch length utilizing OTR from the target.

## 6. – Conclusions

We have developed a beamline for studying interactions between relativistic electrons and crystals. We designed a compact two-axis goniometer for ultrahigh vacuum use. Two screen monitors were placed downstream of the goniometer to observe the profile of the beam transmitting through the crystal. We evaluated the beam emittance and the Twiss parameters using the Q-scan method and confirmed that the beam emittance was small enough for channeling experiments. We also proposed experiments on channeling radiation and parametric X-ray radiation. The aim of the first proposed experiment is to observe diffracted channeling radiation from planar-channeling electrons. This radiation process has not yet been observed and its observation is awaited. As the first step, beam-profile measurements for the survey of channeling conditions will be initiated at the SAGA-LS.

* * *

We would like to express our appreciation to Dr. A. V. Shchagin for discussions on parametric X-ray radiation. We also would like to thank Drs. S. Koda, K. Yoshida, and T. Tomimasu for encouragement in this work. This work was supported in part by a Grant-in-Aid for Scientific Research (21740217).

REFERENCES

[1] Kumakhov M. A., *Phys. Lett.*, **57** (1976) 17.
[2] Ter-Mikaelian M. L., *High Energy Electromagnetic Processes in Condensed Media* (Wiley-Interscience, New York) 1972.
[3] Yoshida K. *et al.*, *AIP Conf. Proc.*, **879** (2007) 179.
[4] Tomimasu T. *et al.*, *AIP Conf. Proc.*, **879** (2007) 184.
[5] Kaneyasu T., Takabayashi Y., Iwasaki Y. and Koda S., *AIP Conf. Proc.*, **1234** (2010) 583.
[6] Endo I. *et al.*, *Phys. Lett. A*, **164** (1992) 319.
[7] Wille K., *The Physics of Particle Accelerators: An Introduction* (Oxford University Press, Oxford) 2001.
[8] Endo I., Iseki D., Ohnishi T., Moriyoshi C. and Shchagin A. V., *Nucl. Instrum. Methods B*, **217** (2004) 666.
[9] Takabayashi Y., Endo I., Ueda K., Moriyoshi C. and Shchagin A. V., *Nucl. Instrum. Methods B*, **243** (2006) 453.
[10] Nawang S. *et al.*, *J. Phys. Soc. Jpn.*, **75** (2006) 124705.
[11] Takabayashi Y., Ishiji K. and Shchagin A. V., *Plan for Experimental Comparison of Diffracted Virtual and Real Photons Pattern*, in *Abstracts of the International Conference Channeling 2010* (2010).
[12] Baryshevsky V. G. and Dubovskaya I. Ya., *J. Phys. C*, **16** (1983) 3663.

[13] Ikeda T., Matsuda Y., Nitta H. and Ohtsuki Y. H., *Nucl. Instrum. Methods B*, **115** (1996) 380.
[14] Matsuda Y., Ikeda T., Nitta H., Minowa H. and Ohtsuki Y. H., *Nucl. Instrum. Methods B*, **115** (1996) 396.
[15] Yabuki R., Nitta H., Ikeda T. and Ohtsuki Y. H., *Phys. Rev. B*, **63** (2001) 174112.
[16] Korotchenko K. B., *J. Surf. Investig. X-ray, Synchrotron and Neutron Tech.*, **4** (2010) 599.
[17] Korotchenko K. B., Fiks E. I., Pivovarov Yu. L. and Tukhfatullin T. A., *J. Phys.: Conf. Ser.*, **236** (2010) 012016.
[18] Takabayashi Y., *AIP Conf. Proc.*, **1234** (2010) 579.